Document downloaded from:

http://hdl.handle.net/10251/184803

This paper must be cited as:

Carrión García, A.; Genovés, V.; Perez, G.; Bittner, J.; Popovics, J.; Paya Bernabeu, JJ.; Gosálbez Castillo, J. (2021). Effects of slow dynamics and conditioning on non-linear hysteretic material evaluation using impact resonance acoustic spectroscopy. Mechanical Systems and Signal Processing. 150:1-15. https://doi.org/10.1016/j.ymssp.2020.107273

The final publication is available at

https://doi.org/10.1016/j.ymssp.2020.107273

Copyright Elsevier

Additional Information

Effects of slow dynamics and conditioning on non-linear hysteretic material assessment using impact resonance acoustic spectroscopy

A. Carrión[a,*], V. Genovés[b], G. Pérez[a], J. Bittner[c], J. S. Popovics[c], J. Payá[b], J. Gosálbez[a,**]

[a]*Instituto de Telecomunicaciones y Aplicaciones Multimedia (ITeAM), Universitat Politècnica de València, Camino de Vera s/n, Edificio 8B, 46022, València, Spain*
[b]*Instituto de Ciencia y Tecnologìa del Hormigòn (ICITECH), Universitat Politècnica de València, Camino de Vera s/n, Edificio 4G, 46022, València, Spain*
[c]*Department of Civil and Environmental Engineering, University of Illinois, 205 N. Mathews Ave, Urbana, IL 61801, USA*

Abstract

The microstructural features of heterogeneous and porous materials cause unique non-linear dynamic behaviour in such materials. The purpose of this work is to investigate the dynamic response of thermally damaged concrete specimens measured by two different methods: Non-linear Impact Resonance Acoustic Spectroscopy (NIRAS) and new Flipped Accumulative Non-linear Single Impact Acoustic Spectroscopy (FANSIRAS). Specimens were characterised in two different dynamic condition states of the material: relaxed and conditioned. The specimen's relaxed state indicates that no previous dynamic excitation event ocurred. The conditioned state denotes that the specimen has been dynamically tested before. The NIRAS results show that the non-linear, α_f and α_Q, are affected by their previous dynamic history. The recently proposed algorithm, FANSIRAS, extracts from a single resonant signal equivalent results to NIRAS when conditioning the specimen. In this situation, both parameters α_f and α_Q were equivalent. The results suggest that new NDT parameters based on non-linear hysteretic parameters can quantify the damage level of thermally treated mortar specimens.

Keywords:
Non-linear Acoustic Spectroscopy, Mortar thermal damage, FANSIRAS, Slow dynamics, Conditioning, Read number

1. Introduction

Geomaterials, such as rocks, sand, soil or their aggregates, such as concrete, belong to a newly defined class, the so-called Non-linear Mesoscopic Elastic (NME) materials [1]. These materials are characterised by having

*Corresponding author's e-mail address: alcarga4@upv.es
**Corresponding author's e-mail address: jorgocas@dcom.upv.es

a heterogeneous internal structure, whose non-linear response appears to be related to their wide variety of microstructural feature, i.e. micro-cracks, grain contacts, interstices, etc., and become orders of magnitude larger than that shown by classic atomic elastic materials. The non-linear elastic behaviour of NME materials cannot be described by the classic non-linear theory of Landau [2]. Its singularity is reflected in the manifestation of hysteretic behaviour and is evidenced by discrete memory effects during the relaxation processes, denominated in the literature as Anomalous Non-linear Fast Dynamics (FD) and Slow Dynamics (SD), respectively [3] for both quasi-static (stress-strain experiments) and dynamic (resonant-wave experiments) behaviour.

The most widely employed Non-Destructive Testing (NDT) methods for monitoring damage processes in concrete and other cement-based materials have focused on studying the material's non-linear dynamic anomalies given its greater sensitivity than linear ones when global defects are detected early [4]. Ostrovsky and Johnson [5] listed a thorough and wide variety of non-linear response manifestations in quasi-static and especially dynamic laboratory experiments. Some are non-linearity and hysteretic and discrete memory phenomena in both stress-strain experiments: the appearance of new harmonic frequency components, wave cross-modulation amplitudes, resonance frequency shifts, amplitude-dependent losses and slow dynamics in non-destructive procedures [4, 6]. These NDT, which draw upon non-linear dynamic behaviour, are considered to be Non-linear Elastic Wave Spectroscopy (NEWS) methods.

Regardless of the source used to excite the specimens under study, all NEWS methods share the same baseline concepts for extracting the characteristic non-linear parameters of mesoscopic materials for evaluating cracks, voids and defects. Thanks to its easy excitation procedure and remarkable sensitivity reached when measuring non-linear behaviour, a prominent research line focuses on impact spectroscopy. Conversely to the multiple energy increasing impact driving amplitudes needed in the Non-linear Impact Resonance Acoustic Spectroscopy (NIRAS) methodology [7–9] to quantify the non-linear response, recent advances have centred on single impact approaches based on an optimal signal processing procedure [10, 11]. Accordingly, a novel single impact technique, FANSIRAS, has recently been introduced to characterise the underlying non-linear physical phenomenon from a signal processing perspective [12]. Following the application of upward/downward protocols to evaluate hysteresis and effects of conditioning proposed in [13] for ultrasonic experiments and their influence on the measurements

proposed in [14] for Non-linear Resonance Ultrasonic Spectroscopy (NRUS), a comparison of both techniques, NIRAS and FANSIRAS, is taken a step further in the present study. Both approaches are applied to two different motion process moments of specimens, resting (a rested specimen is excited by impacts whose level consecutively increases) and conditioned (a rested specimen is excited by impacts whose level consecutively decreases), to assess the effects of slow dynamics and conditioning on the impact resonance spectroscopy techniques. The joint analysis of both configurations (upward- and downward-energy impacts) may describe the hysteretic behaviour of non-linear mesoscopic materials like mortar or concrete.

Damage in concrete has been widely investigated over the years from many points of view. Different degradation mechanisms cause distinct modifications to the material dynamic response, which means having performed a detailed analysis of all the physical mechanisms to fully understand degradation processes [15–17]. Thermal damage in concrete particularly depends on many variables, of which the most important are the composite dose (aggregate type and proportion, water/cement ratio, cement type, etc.) and exposured temperature. Given the complexity of this damage (stiffness matrix loss, incompatibility of deformation between aggregate and paste, expansive products, etc.), several studies have been carried out to distinguish and quantify damage and the material's physical behaviour [18, 19]. In order to assess this degradation process, NDT evaluations through ultrasonic inspection and vibrational analysis are the most widespread and developed techniques for their simple implementation and non-invasive nature [8, 9, 20–23]. Moreover, several studies have analysed the case of thermal damage in concrete by NEWS techniques. Such studies have monitored the effect of thermal damage in concretes by evaluating non-linear acoustic parameters by means of NIRAS [24] and Non-linear Resonance Ultrasonic Spectroscopy (NRUS) [8, 25–27]. These studies have also run distinct tests to support the non-linear acoustic results by means of apparent expansion determinations [27], semi-quantitative analysis on paste-aggregate images [25] and ultrasonic pulse velocity measurements [8, 27]. One work has been recently published that correlates such additional tests and non-linear parameters to determine the spoiling process of mortar, but by analysing loss of stiffness of the cement matrix and the aggregate debonding mechanism as a joint degradation phenomena in the thermal damage of mortar [28].

In the present study, the authors implement a vibrational analysis that considers the non-equilibrium dynamics

of mortar elements under stepped thermal damage. This analysis permits to simultaneously draw upon the whole potential of the NEWS techniques, and to assess the robustness of the non-linear parameters extracted with NIRAS and FANSIRAS against the effects of slow dynamics and conditioning at different damage levels. In the present study, the authors implement vibrational analyses that consider the non-equilibrium dynamics of mortar elements subject to stepped thermal damage. These analyses provide deeper understanding of the robustness of non-linear parameters extracted with NIRAS and FANSIRAS methods considering significant effects of slow dynamics and conditioning that, if ignored, may result in significant discrepancy among these and other NEWS measurements.

2. Mathematical background

The classic theory of non-linear elasticity is unable to describe the elastic behaviour of non-linear mesoscopic elastic materials [29, 30]. In particular, their stress-strain relation has to be developed in such a way that the terms describing hysteresis and discrete memory are taken into account [31]. In this context, the one-dimensional stress-strain relation can be expressed as:

$$\sigma(\varepsilon) = K_0\left(1 + \beta\varepsilon + \delta\varepsilon^2 + \dots\right) + H[\varepsilon, \mathrm{sign}(\dot{\varepsilon})] \tag{1}$$

where σ is stress, ε is strain, K_0 is the linear elastic modulus, β and δ represent the classic quadratic and cubic non-linear parameters, respectively, which can be developed as a combination of second-, third- and fourth-order elastic constants [2, 32], H is a function describing the hysteretic relation between σ and ε, and $\dot{\varepsilon}$ is the strain rate [30, 31, 33]. Several models exist for the description of function H in Eq. 1. The hysteretic quadratic non-linearity model [30, 33] (Eq. 2) provides the opportunity to develop analytical approaches and is sufficiently realistic to explain some important manifestations observed in hysteretic materials:

$$H[\varepsilon, sign(\dot{\varepsilon})] = \alpha(\Delta\varepsilon + \varepsilon \cdot \mathrm{sign}(\dot{\varepsilon})) \tag{2}$$

where α is a measure of material hysteresis. Indeed by substituting in the wave equation and calculating the non-linear contribution to the solution, we find a linear decrease in resonance frequency for increasing strain levels, a quadratic amplitude dependence of the third harmonic and a linear increase of the modal damping ratio (decrease in the quality factor). This model is functional, but its original formulation accounts for neither slow

dynamics, the recovery process that occurs in these materials after large amplitude wave excitation, nor for the conditioning process, strain-memory that takes place while applying resonance experiments [3, 31, 34].

The resonant acoustic spectroscopy method has been traditionally used to assess mechanical engineering properties, such as the elastic moduli and material damping. A discrete resonant acoustic reverberation signal, $y(n)$, may be modelled as a damped harmonic oscillator, which is mathematically described by the product of an exponentially decaying function, $a(n)$, and an exponentially time-varying phase signal, $s(n)$ [12, 35, 36]:

$$y[n] = a[n] \cdot s[n] = \left(A \cdot e^{-\gamma n T_S}\right) \cdot \left(sin\left(2\pi f_0 n Ts + \phi[n]\right)\right), n \in \{0, \ldots, N-1\} \tag{3}$$

where A denotes amplitude, γ is attenuation, f_0 is linear frequency and $\phi(n)$ is the time-varying phase. T_S is the sampling period and N is the number of samples acquired in the sampling interval. Figure 1a shows a typical discrete resonant acoustic reverberation impact signal in the time domain, where the characteristic decreasing exponential amplitude is seen at a glance. The signal's resonant frequency and damping characteristics are extracted from the spectral domain in the region surrounding the resonant frequency peak (Figure 1b). The frequency domain is obtained by applying the discrete-frequency Fourier Transform (DFT) with equally spaced frequency points (N_{DFT}):

$$Y[f] = T_S \cdot DFT\{y[n]\} = T_s \cdot \sum_{n=0}^{N_{DFT}-1} y[n] \cdot e^{-j2\pi f n T_S}, f \in [0, f_S/N_{DFT}, \ldots, (N_{DFT}/2-1) \cdot f_S/N_{DFT}] \tag{4}$$

The resonant frequency peak depends on the sample's dimensions, mass and the dynamic modulus related to the material's elastic properties. The material's damping capacity is determined from the quality factor, Q (or inverse attenuation), which represents the ratio between the elastic energy stored at maximum stress and strain during harmonic excitation, and the energy loss per cycle, related to the material's dissipative capacity [3].

2.1. NIRAS

The Non-linear Impact Resonance Acoustic Spectroscopy (NIRAS) technique relies on an impulse excitation of the specimen repeated with different impact strengths. The different reverberation signals are denoted by $y_i(n)$, where i is the impact number (in this study, $i \in [1, 10]$ where $i = 1$ corresponds to the first level of impact and $i = 10$ corresponds to the latest level of impact). The non-linear parameter related to resonance frequency shift

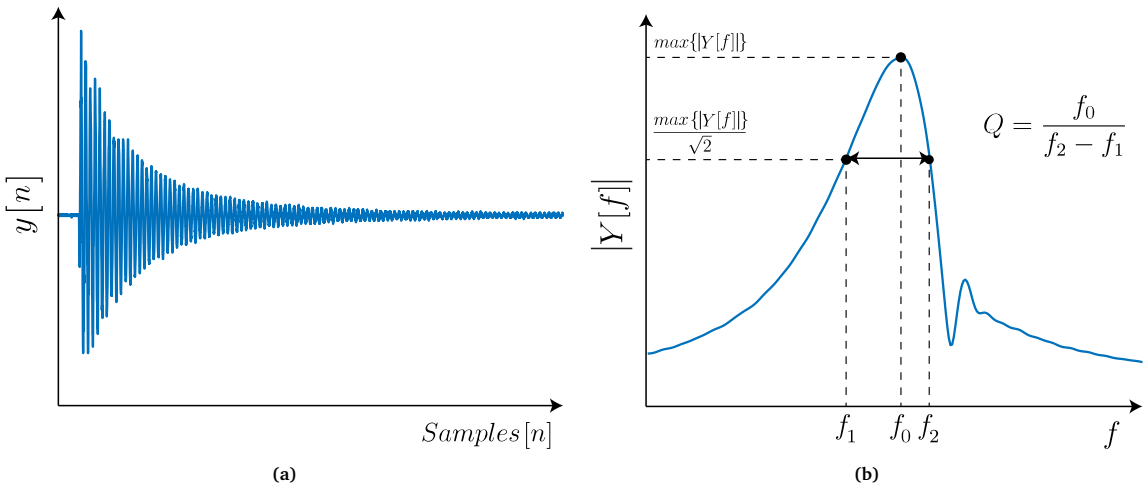

Figure 1: a) Temporal domain representation of a typical discrete resonant acoustic reverberation signal, $y(n)$. b) Frequency domain representation of a typical discrete resonant acoustic reverberation signal, $Y[f]$.

α_f^{NIR} is obtained from a linear regression fit:

$$\frac{\tilde{f}_0 - \tilde{f}_i}{\tilde{f}_0} = \alpha_f^{NIR} \cdot A_i \tag{5}$$

where A_i is the obtained peak amplitude spectrum (Fig. 1b)

$$A_i = max\{|Y_i[f]|\} \tag{6}$$

and $\tilde{f}_i$ is the peak normalised frequency of one mode (Fig. 1b)

$$\tilde{f}_i = max_f\{|Y_i[f]|\} \tag{7}$$

from the multiple impacts at different strengths i. Here $\tilde{f}_0$ denotes the resonance frequency obtained in the linear strain regime. For low excitation amplitudes [37], the frequency shift $(\tilde{f}_0 - \tilde{f}_i)$ is non-existent and the peak frequency is considered to be obtained in the linear strain regime. In this study, $\tilde{f}_0$ is determined as the intersection with the y-axis of the linear relation between peak amplitudes A_i (x-axis) and peak frequencies $\tilde{f}_i$ (y-axis)(Figure 2). The non-linear parameter related to the shift of the damping properties, α_Q^{NIR}, is assumed to also exhibit a linear relation (Eq. 8):

$$\frac{1}{Q_i} - \frac{1}{Q_0} = \alpha_Q^{NIR} \cdot A_i \tag{8}$$

where A_i is the peak amplitude (Eq. 6), and Q_i is the damping factor obtained for each impact i (Eq. 9)

$$Q_i = \frac{\tilde{f}_i}{\tilde{f}_{i,2} - \tilde{f}_{i,1}} \tag{9}$$

where $\tilde{f}_{i,2} - \tilde{f}_{i,1}$ is the half-power bandwidth resonance (Fig. 1b), and Q_0 is the linear regime damping factor determined as the intersection with the y-axis of the linear relation between the peak amplitudes A_i (x-axis) and the measured damping factors Q_i (y-axis, Figure) [21]. An increase in both parameters, α_f^{NIR} and α_Q^{NIR}, is expected that is proportional to the hysteresis α in Eq. 2 when the specimen's thermal damage.

Parameters α_f and α_Q measure the importance of the elastic and dissipative hysteretic effects, respectively [38]. In order to characterise the relative changes of resonance frequency and Q with strain level, the Read ratio (α_Q/α_f) is introduced [39, 40]. Note that this parameter equals 1 in the approximation of the purely quadratic hysteretic nonlinearity theoretically predicted by models such as the P-M space [3, 41].

2.2. FANSIRAS

The technique called Flipped Accumulative Non-Linear Single Impact Resonance Acoustic Spectroscopy (FANSIRAS) only requires a single reverberation signal $y_I[n]$, plus suitable optimal signal processing to obtain a reliable non-linearity estimate. The method can be described as a window of initial length that equals that of the acquired signal, N, whose length progressively shortend to the lower bound, and transforms the time segment of the impact signal within the p-th window, $y_{I,w_p^{L_p}}[n]$, into the frequency domain at each window position:

$$y_{I,w_p^{L_p}}[n] = y_I[n] \cdot w^{L_p}[n - p \cdot M], \qquad n \in \{0, \ldots, N-1\}, p \in \left\{0, \ldots, \left\lfloor \frac{N}{M} \right\rfloor - 1\right\} \tag{10}$$

Here $w_p^{L_p}[n]$ represents a rectangular window, which shortens in each algorithm step:

$$w_p^{L_p}[n] = \begin{cases} 1, & 0 \le n \le L_p - 1 \\ 0, & otherwise \end{cases} \tag{11}$$

The length of the window varies at each position p, $L_p = N - p \cdot M$, where M represents the number of samples by which the window decreases in each algorithm step. The number of points used in the later regression is related

to M value, but does not significantly affect the estimation of the non-linear parameters. In this work, M equals the number of samples during two periods of the signal ($M = 2f_s/\tilde{f}_0$, where f_s is sampling frequency).

Non-linear parameters $\alpha_{f,I}^{FAN}$ and $\alpha_{Q,I}^{FAN}$ are both estimated according to the linear fits seen for NIRAS, but using the current variables obtained from a single reverberation signal corresponding to the strongest impact level I.

Each time segment of the reverberation signal within the $p-th$ window, $y_{I,w_p^{L_p}}[n]$, is studied in the frequency domain by applying the discrete-time discrete-frequency Fourier Transform (DFT), which results in $Y_{I,w_p^{L_p}}[f]$:

$$Y_{I,w_p^{L_p}}[f] = DFT\{y_{I,w_p^{L_p}}[n]\} \tag{12}$$

For each position p, the peak amplitude spectrum $A_{I,p}$ is computed (Eq. 13)

$$A_{I,p} = max\{|Y_{I,w_p^{L_p}}[f]|\} \tag{13}$$

and peak frequency $\tilde{f}_{I,p}$ (Eq. 14)

$$\tilde{f}_{I,p} = max_f\{|Y_{I,w_p^{L_p}}[f]|\} \tag{14}$$

where function $max_f\{\cdot\}$ defines the peak amplitude spectrum projected over the frequency vector. The non-linear parameter related to the resonance frequency shift $\alpha_{f,I}^{FAN}$ is obtained from the linear fit of $A_{I,p}$ and $\tilde{f}_{I,p}$ (Eq. 15)

$$\frac{\tilde{f}_{I,0} - \tilde{f}_{I,p}}{\tilde{f}_{I,0}} = \alpha_{f,I}^{FAN} \cdot A_{I,p} \tag{15}$$

where $\tilde{f}_{I,0}$ is the resonance frequency obtained in the linear strain regime. $\tilde{f}_{I,0}$ is determined as the intersection with the y-axis of the linear relation between peak amplitudes $A_{I,p}$ (x-axis) and peak frequencies $\tilde{f}_{I,p}$ (y-axis).

Analogously, damping factor $Q_{I,p}$ is also computed for each $p-th$ window position (Eq. 16):

$$Q_{I,p} = \frac{\tilde{f}_{I,p}}{\tilde{f}_{I,p,2} - \tilde{f}_{I,p,1}} \tag{16}$$

and the non-linear parameter proportional to the damping properties $\alpha_{I,Q}^{FAN}$ is obtained as the slope of the linear relation between the peak amplitudes, $A_{I,p}$, and the damping factor, $Q_{I,p}$:

$$\frac{1}{Q_{I,p}} - \frac{1}{Q_{I,0}} = \alpha_{I,Q}^{FAN} \cdot A_{I,p} \tag{17}$$

where $Q_{I,0}$ is the approximation for the linear regime damping factor related to reverberation signal $y_I[n]$. When working with real signals (N samples acquired with a sampling frequency f_s), window shortening must stop before losing any signal information (exceedingly small window). To halt a stop condition, the window in the FANSIRAS algorithm is decreased until the Q value is lower than that obtained in the previous window. See [12] for further technical aspects of the algorithm. In the following sections, the Read ratio estimated from $\alpha_{I,f}^{FAN}$ and $\alpha_{I,Q}^{FAN}$ is also analysed.

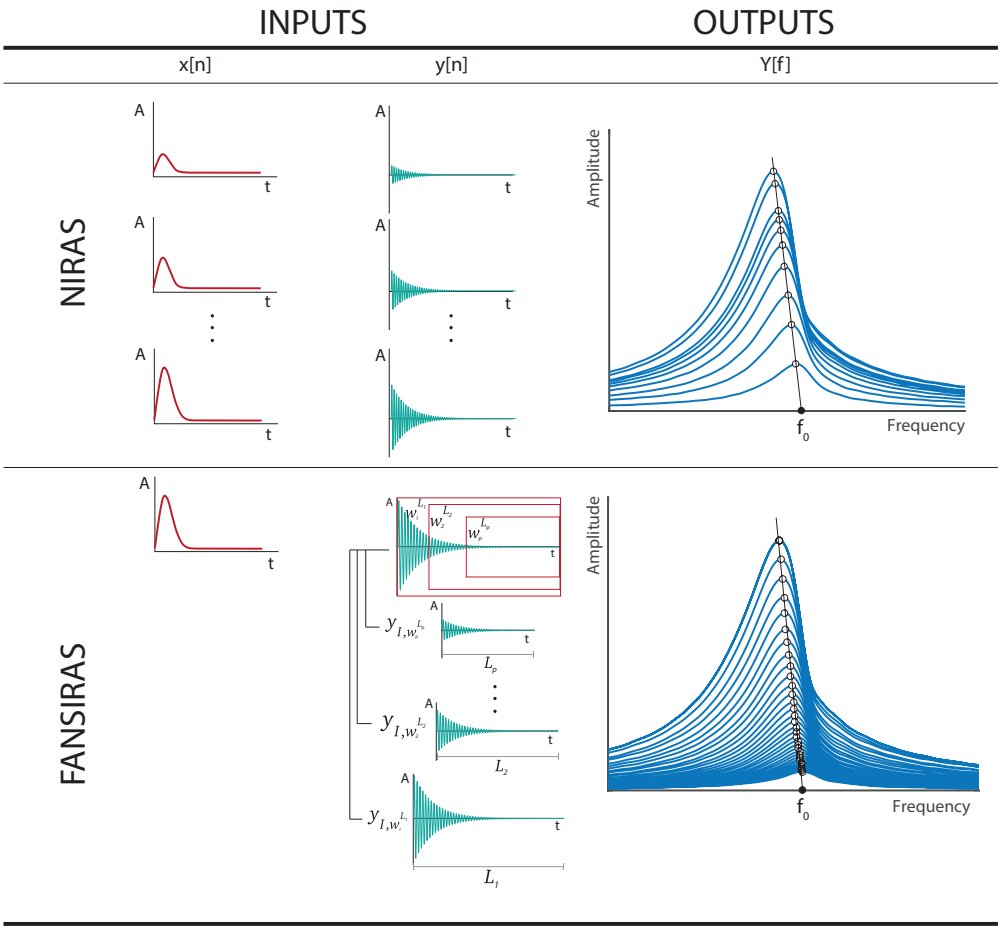

Figure 2: Schematic comparison between techniques NIRAS and FANSIRAS. The NIRAS algorithm (top) is represented by 10 impact signals with varying input force amplitudes $x_i[n], i \in [1, 10]$, and its corresponding output reverberation signals, $y_i[n], i \in [1, 10]$, and their corresponding Fourier Transform spectra, $Y_i[f]$. The FANSIRAS algorithm (bottom) reconstructs the equivalent NIRAS signals from a single output reverberation signal, $y_I[n]$, by means of signal processing.

Figure 2 shows a schematic representation of the two algorithms in both the time and frequency domains. It summarises the differences between the procedures distinguished mainly by the number of input signals (number of blows) and signal processing. NIRAS uses 10 measurements with varying impact force amplitudes, while

FANSIRAS requires only one measurement at a high impact force amplitude. The FANSIRAS signal processing algorithm attempts to reconstruct NIRAS technique signals in order to extract equivalent non-linear parameters from a single measurement.

3. Experimental

3.1. Materials and specimens

Six mixes of standardised Portland cement mortar (water/cement = 0.5), made of 450 g of Spanish cement CEM I-52.5-R, 1350 g of 0/2 mm crushed quartz sand and 225 g of water, were prepared to obtain eighteen $40 \times 30 \times 160$ mm^3 specimens. After the mixing process, iron moulds were stored in the wet chamber (20°C and 100% H.R.) for 24 hours. Then, the 18 mortar test samples were demolded and stored in the wet chamber for an additional 60 days (beyond the 28 standard days) so that the elastic property changes caused by hydration were as constant/stable as possible. Afterwards, specimens were dried at 40°C for 7 days. Then samples were wrapped in plastic film until room temperature was reached once again to characterise them in what we define to be the pristine state. Two thermal damage treatment levels were applied according to the chemical decomposition of Portland cement hydrates. The first level contained six specimens that were thermally damaged at 400°C (C-S-H and C-A-H decomposition took place), and this temperature was reached in 2 hours, kept for 3 hours and slowly cooled for 12 hours inside an oven. The second level contained six specimens that were thermally damaged at 525°C ($Ca(OH)_2$ decomposition took place) following the same procedure as mentioned for the 400°C damaging test. In this way, six different specimens per condition (40, 400 and 525°C) were created to carry out the non-linear acoustic analysis. Three additional specimens per series were manufactured to run traditional destructive tests. In the first instance, mortar blocks were tested in a three-point bending test configuration to obtain the flexural strength of the material exposed to 40, 400 and 525°C. The remaining six semi-prisms were used to obtain compressive strength. Two other specimens heated at 400°C were also prepared to carry out the reproducibility test described in Section 4.2.1. The aforementioned manufacturing process is the same as in [12], but different samples were tested in each research work.

3.2. Test Layout

Acoustic resonance tests were carried out for the 18 specimens in the three thermal treatments. The experimental layout comprise an impact hammer (Brüel & Kjær 8206-003) attached to an iron axle located in a metallic structure. This metallic axle was supported on two ball bearings that yield free rotational motion on one plane with minimal friction. The specimen was located on slightly sloping metallic supports to allow allowing a centred and perpendicular impact on the specimen's face. On the opposite face to the impact, in the top-left corner, a piezoelectric accelerometer sensor (PCB 352A21) was attached to obtain the vibrational motion of the test probe. The electric signal of the instrumented hammer and the accelerometer went through a signal conditioner (PCB 482A18) by transmitting it to the oscilloscope (Tektronix MDO3014). The oscilloscope was configured with f_s equalling 250 kHz, N equalling 10000 samples, the trigger voltage equalling to 120 mV and the pretrigger time equalling 1 ms. Finally, the information was transmitted via USB to a computer with a control software developed by the authors based on the Instrument Control Toolbox of MATLAB. The amplitude of the impacts used in the experiment allowed us to work in the non-linear regime of the tested specimens, but still well within the linearity limits of the set-up (accelerometer, signal conditioner and oscilloscope). Figure 3 shows the amplitude of the impact events that comprise one NIRAS test. Note that the impact load amplitudes vary between 20N and 70N for a 400°C damaged specimen. These values vary slightly depending on the material's stiffness.

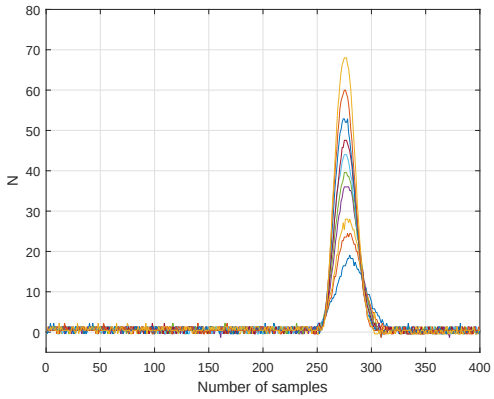

Figure 3: Impact signals applied for one NIRAS test. Signals registered by the instrumented hammer Brüel & Kjær 8206-003 on a 400°C damaged specimen.

4. Results and Discussion

4.1. Mechanical and physical properties of mortar

The compressive strength results are shown in Figure 4a. The compressive strength at 40°C, 62.5±4 MPa was slightly higher than the corresponding value for this dose type and cement type (52.5 MPa) due to the treatment at 40°C. For 400°C, a value of 55±3 MPa was obtained, with minor variation (reduction of 12%) from the initial value due to the stiffness loss of the matrix and the degradation of the interfacial transition zone between the paste and the aggregate. At 525°C, compressive strength dramatically dropped and 27±2 MPa was obtained, which means that it lost at least 56 % of its initial strength. A similar trend in performance was found for flexural strength (Figure 4b). This parameter was more sensitive to thermal damage than compressive strength because spoiled interfaces, micro-cracks and defects were expected to be partially stressed with a tensile load. Reductions in flexural strengths of 40% and 90% were observed for the 400 and 525°C treated samples respectively. In the compressive test, such defects were compressed, which allowed withstanding higher stress than the tensions produced by the flexural test. Figure 4c shows the dynamic modulus values calculated from the first flexural mode of the mortar specimens following Standard ASTM C-215. In this plot, a linear decay of the material's stiffness is observed. The linear modulus was related to the state of the cement matrix. Therefore with thermal damage, hydration products were lost during this process until complete portlandite decomposition took place (>550°C).

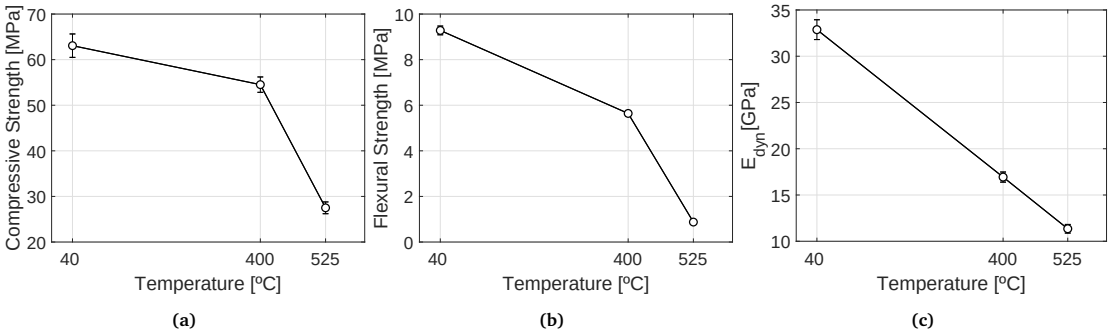

Figure 4: Mechanical properties according to exposure temperature: a) compressive strength. b) flexural strength. c) transversal dynamic elastic modulus.

4.2. Resonance Techniques based on Impact Spectroscopy

4.2.1. Reproducibility Test

The discrete memory effects of hysteretic behaviour have been reported in several studies [3, 42]. Impact spectroscopy techniques rely on the impact of a specimen at different amplitude. Thus the importance of the order

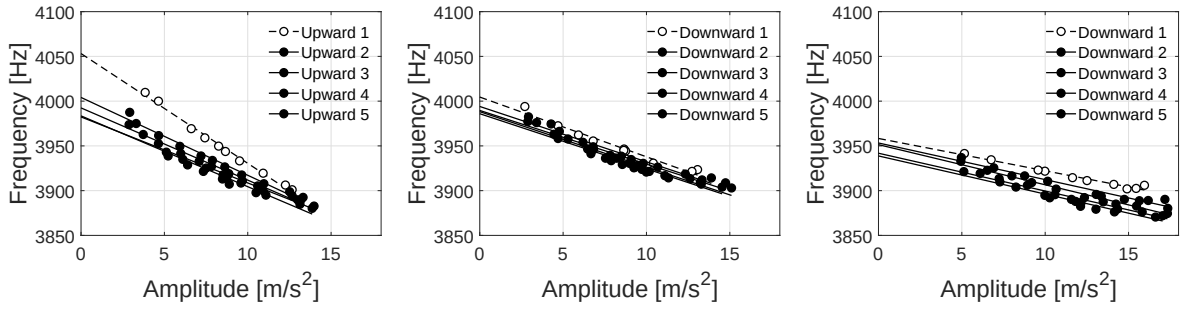

Figure 5: Reproducibility Test. Five repetitions of the resonance tests (10 different amplitude impacts) on two different specimens damaged at 400°C: A and B. a) Upward configuration (starting with the lowest energy impact) on specimen A. b) Downward configuration (starting with the highest energy impact) on specimen A. c) Downward configuration on specimen B.

of blows and their intensity must be taken into account. In line with this, two different configuration tests were set up: upward configuration, 10 blows progressively increasing the impact energy; and downward configuration, 10 blows decreasing the impact energy. 10 impacts represent a balance between a sufficiently high number of data to enable accurate linear regression and a sufficiently low number of impacts to avoid causing residual harm to the sample surface. In order to analyse the repeatability of tests, five consecutive repetitions of the tested configuration were done.

Two different specimens damaged at 400°C were tested: specimen A and B. Five consecutive NIRAS tests for the upward configuration were applied to specimen A. The results are shown in Figure 5a. Two different trends were easily identified: the first test (dashed line) showed a different slope to the remaining four tests (solid lines). Despite being parallel, lines differed on the y-axis intersection. This plot gave a graphical understanding of the anomalous non-linear concepts introduced into Section 1: fast dynamics, slow dynamics and conditioning. The linear regression slope, indicated by the amplitude-dependent frequency shifts, represented the fast dynamics behaviour, which was constant from the second upward test. The decreasing intersection of each consecutive test with the y-axis represented the discrete memory, which was a manifestation of slow dynamics. The particular trend shown by the first test (dashed line) denoted the behaviour of the specimen without conditioning when relaxed. Having conditioned the specimen, and after a series of blows, the observable trends were indicated by solid lines. The specimen was conditioned in fast dynamics terms (the slope of the linear fit was constant), but the slow dynamics conditioning continued by decreasing the linear resonance frequency in each consecutive experiment.

As the memory recovery time follows $log(t)$ dependence [43], test sample A was left undisturbed for 48 hours to ensure the material's a consistent initial relaxed state. The majority of the idealised memory recovery was achieved during the 48 hour rest period. Figure 5b plots the obtained results in the downward configuration for specimen A. In this case, the specimen was completely conditioned from the very first and strongest impact, and a constant trend was observed for the five tests. Even though the specimen had relaxed, the linear regression from the downward configuration allowed the identification of the same slope and y-axis interception as in the upward configuration after being conditioned.

In order to avoid any doubt about the recovery time, five consecutive NIRAS tests with the downward configuration were applied to specimen B, which had never been tested before. The obtained results are plotted in Figure 5c. Although the specimen was relaxed, it was completely conditioned from the first and strongest impact. The observable behaviour coincided with the unique trend seen in Figure 5b. In order to fully characterise the thermal damage given by the previous results, specimens were tested using the two established configurations, an upward and a downward test, land a 48 hours resting time was allowed between tests. After each test the specimens were always left in the wet chamber in order to control the ambient conditions.

4.2.2. NIRAS and FANSIRAS analyses

In the present section, non-linear parameters α_f and α_Q obtained by both techniques NIRAS and FANSIRAS are shown for three representative mortar samples in three different thermal damage stages(40°C, 400°C and 525°C). Firstly, the two techniques for both configurations were compared to estimate the different trends that arose from the conditioning effect, and how it evolved with the increasing deterioration degree of specimens. Figure 6 shows the signal amplitude effect on the resonance frequency for each damage level. We can see that the largest resonance frequency significantly dropped as damage increased (5660 Hz, 40°C; 4000 Hz, 400°C; and 3450 Hz, 525°C). For the three damage level, NIRAS and FANSIRAS (estimated on the strongest impact of the NIRAS technique) identified two different trends in the upward configuration (upper row in Figure 6). On the contrary, both the algorithms applied to the downward configuration resulted in a unique trend, which coincided with the upward FANSIRAS trend. Table 1 summarises the numerical values of α_f obtained by both algorithms NIRAS and FANSIRAS, and in each configuration.

The differences between the NIRAS upward configuration and the NIRAS downward configuration could be proportional to the system's degree of conditioning between the resting state and the conditioned state. This difference among trends increased as the applied thermal treatment damaged the mortar matrix. Note that the NIRAS algorithm had a limited number of amplitude values depending on the hardware involved in the experiment, but FANSIRAS processing allowed to increase the measurable dynamic range from smaller peak amplitudes to the same largest value.

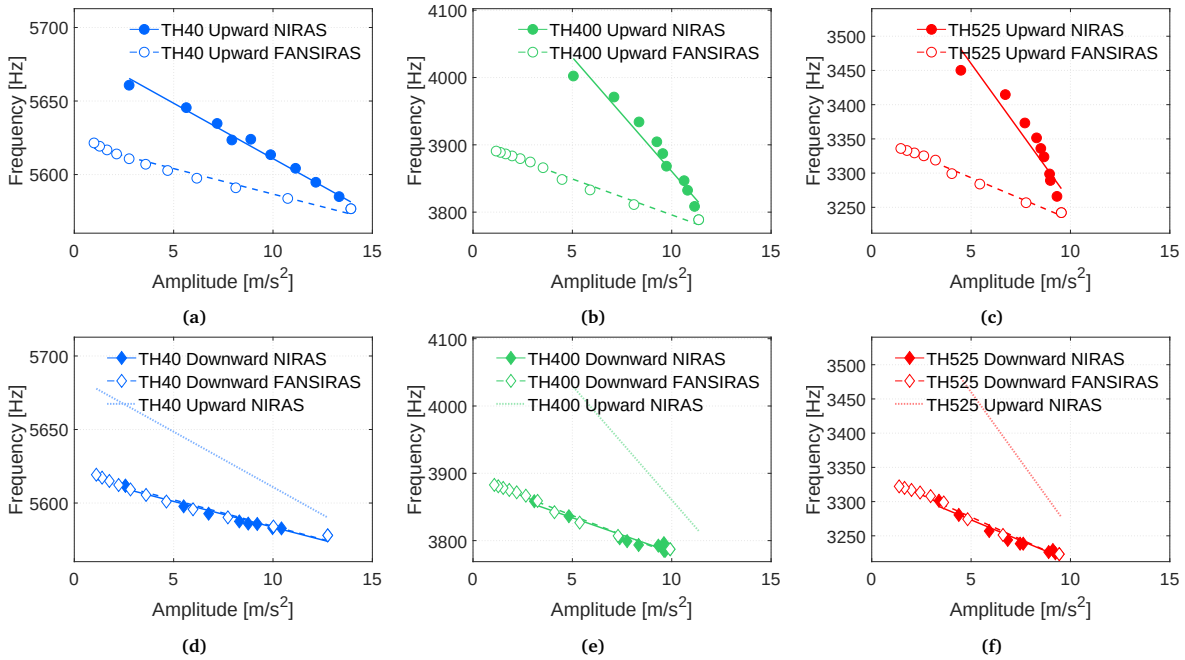

Figure 6: Representative results of the relative resonance frequency shift (α_f) at the different exposure temperatures computed by the NIRAS technique (filled markers and solid lines) and the FANSIRAS technique (hollow markers and dashed lines) and for the two different analysed configurations: upward impact amplitudes (upper row) and downward impact amplitudes (below row). a) 40°C (blue), b) 400°C (green) and c) 525°C (red). Table 1 summarises the numerical α_f values obtained by both algorithms NIRAS and FANSIRAS, and in each configuration.

Analogously, Figure 7 shows the amplitude-dependence for damping factor Q for each damage level. As the damage increases, the maximum value of the damping factor rose. The fact that the normalised peak frequency decreased with increasing drive levels, and the resonance peak simultaneously broadened, indicates that the material non-linear dissipation increased with material softening [44]. Once again, different trends between the NIRAS upward and FANSIRAS upward configurations were easily identified (upper row in Figure 7). Both the algorithms applied to the downward configuration showed similar trends (bottom row in Figure 7). The FANSIRAS estimations slightly differed from the NIRAS estimations because of the changes on the amplitude

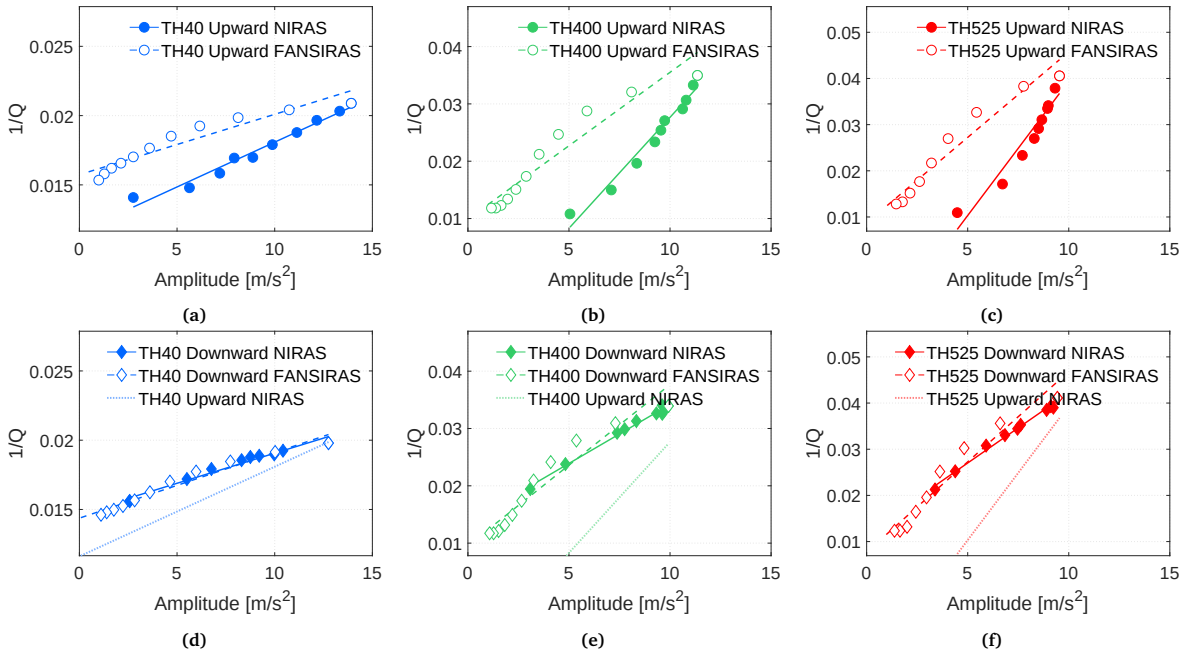

Figure 7: Representative results of the amplitude dependent damping factor (α_Q) at the different temperatures computed by the NIRAS technique (filled markers and solid lines) and the FANSIRAS technique (hollow markers and dashed lines), and for the two different analysed configurations: upward impact amplitudes (upper row) and downward impact amplitudes (below row). a) 40°C (blue), b) 400°C (green) and c) 525°C (red). Table 1 summarises the numerical α_Q values obtained by both algorithms NIRAS and FANSIRAS, and in each configuration.

Table 1: Numerical results of a representative sample of the relative resonance frequency shift (α_f) and the amplitude dependent damping factor (α_Q) at the different exposure temperatures (40°C, 400°C and 525°C) computed by the NIRAS technique and the FANSIRAS technique, and for the two different analysed configurations: upward impact amplitudes and downward impact amplitudes. Each α value also has its corresponding coefficient of determination (R^2) obtained from the linear fit.

Sample	TH40		TH400		TH525	
α ($\times 10^{-3}$)	Upward	Downward	Upward	Downward	Upward	Downward
α_f^{NIR} (R^2)	1.3 (0.98)	0.6 (0.96)	8.5 (0.94)	2.7 (0.95)	12.8 (0.93)	3.1 (0.95)
α_f^{FAN} (R^2)	0.6 (0.97)	0.6 (0.97)	2.7 (0.98)	3 (0.98)	4 (0.98)	4.1 (0.98)
α_Q^{NIR} (R^2)	0.6 (0.97)	0.4 (0.97)	3.9 (0.96)	2.1 (0.99)	6.4 (0.97)	2.9 (0.98)
α_Q^{FAN} (R^2)	0.4 (0.90)	0.4 (0.96)	2.6 (0.91)	2.8 (0.92)	3.8 (0.93)	3.9 (0.91)

ranges and the loss of linearity in the regression fit as the damaged increased. This difference could be related to the nature of the signals used in each spectroscopy technique. The NIRAS technique estimates non-linear parameters from several original reverberation signals, but the FANSIRAS algorithm estimates the different strain levels from a single relaxing signal. Table 1 summarises all the numerical α_Q values obtained by both algorithms NIRAS and FANSIRAS, and in each configuration, upward and downward, for three representative specimens

exposed to different damage treatments. It also presents the R^2 values for each regression.

The response of the dynamic parameters to the different ways in which specimens were excited indicates the crucial importance of choosing between one configuration and another. It is important to understand the differences obtained by the NIRAS and FANSIRAS algorithms and each configuration. Before applying the NIRAS upward configuration, the specimen was stated to be relaxed. Progressively increasing the amplitude of impacts led to the progressive conditioning of the sample under study. Therefore, the NIRAS algorithm applied to an upward configuration quantified the non-linear parameters from different conditioning states.

Conversely for the NIRAS applied to a downward configuration, the specimen was conditioned from the first and largest driving impacts, which isolated the hysteretic parameter from any non-equilibrium in the material's elastic response of the material. The robustness of the FANSIRAS technique, by virtue of using a single impact, was proved against different conditioning states and, therefore, seemed an equivalent regardless of the applied configuration (upward or downward). Therefore, conditioning the sample before taking non-linear measurements, or using a robust algorithm against it such as FANSIRAS, could be a method for separating effects owing to the non-linearity of those due to non-equilibrium effects [45].

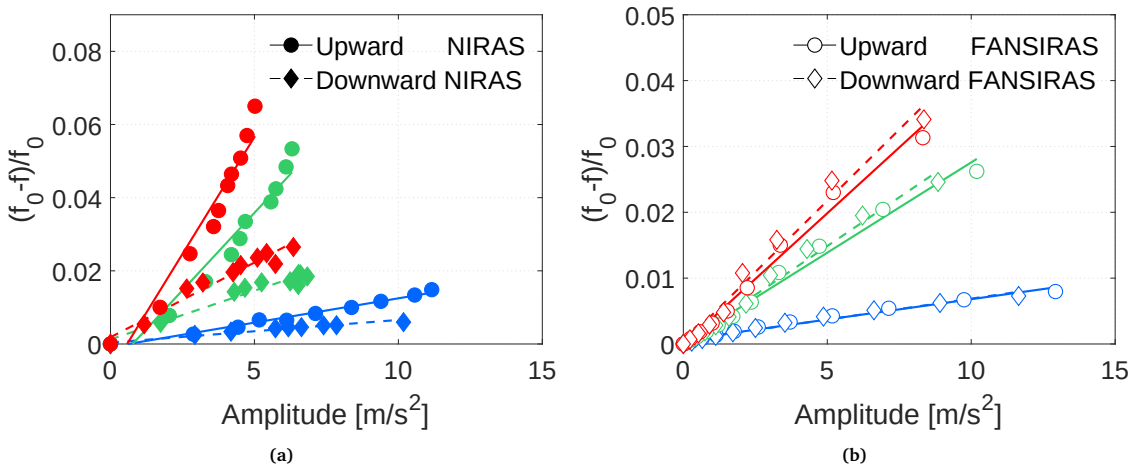

Figure 8: Representative results of the normalised relative amplitude-dependent damping factor (α_f) at different exposure temperatures: 40°C (blue), 400°C (green) and 525°C (red) computed by a) the NIRAS technique (filled markers) and by b) the FANSIRAS technique (hollow markers), and for the two different analysed configurations: upward impact amplitudes (solid lines) and downward impact amplitudes (dashed lines).

Once the conduct influenced by the test configuration was known, the set of resonance frequencies and damping factor values obtained by NIRAS and FANSIRAS were normalised by their values in the linear strain regime. With these normalised values, comparable outcomes were obtained, and different thermal level responses

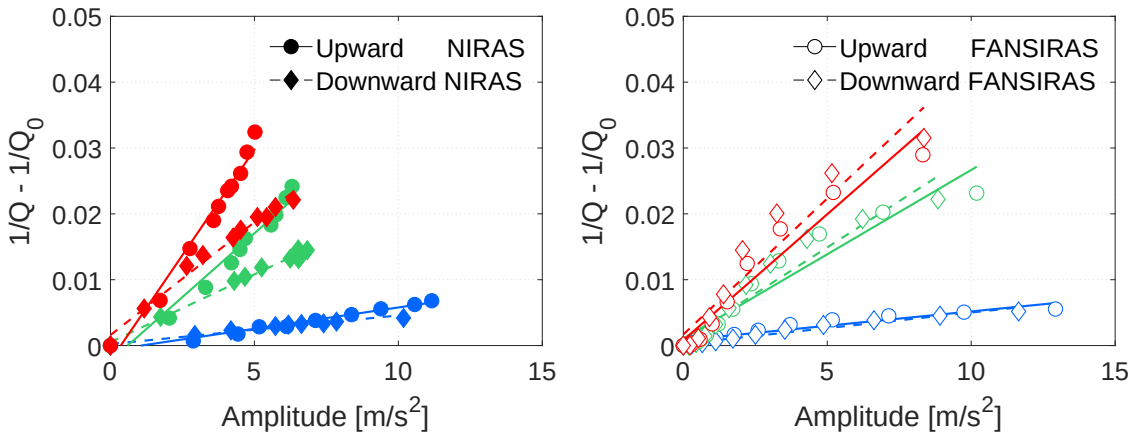

Figure 9: Representative results of the normalised relative amplitude-dependent damping factor (α_Q) at different exposure temperatures: 40°C (blue), 400°C (green) and 525°C (red) computed by a) the NIRAS technique (filled markers) and b) the FANSIRAS technique (hollow markers), and for the two different analysed configurations: upward impact amplitudes (solid lines) and downward impact amplitudes (dashed line).

and techniques were compared. In Figure 8a, the NIRAS excited with the upward configuration displays larger non-linear parameters than those obtained with the downward configuration, and FANSIRAS for either of the two proposed configurations, as shown in Figure 8b. The small differences between FANSIRAS data collected using the upward and downward configurations, respectively, are likely because the data were collected from the same specimen but with measurements spaced 48 hours apart. Small differences in ambient laboratory temperature and moisture content within that 48- hour span may have occurred. With no knowledge about the specimen impact history, lack of consistency between previous states could lead to failure in the damage level classification (see NIRAS TH400 upward and TH525 downward in 8a).

Figure 9a also shows the conditioning effects on the damping factor estimation done by the NIRAS algorithm, albeit with a weaker influence that for the amplitude-dependent frequency parameter (Figure 8a). This behaviour could be related to the nature of the Q parameter of a signal drawn by a harmonic damped oscillator, where the quality factor was the ratio between the system energy and the used energy. Such a ratio seemed more robust against the conditioning of the specimen impact after impact. Besides the steadiness shown when applying the FANSIRAS technique, regardless of the excitation configuration employed (Figures 8b and 9b), the thermal damage characterisation in each tested stage still showed reliable sensitivity.

In order to analyse the consistency of the non-linear parameter values along with increasing thermal damage, the estimation of parameters α_f and α_Q with a bigger number of samples (6 of each for the proposed thermal

damage for a total of 18 specimens) is shown in Figure 10.

Figure 10a depicts the resonance frequency shift amplitude-dependent parameter (α_f) in the same fashion as Figure 10b shows it for the damping factor response (α_Q). Apart from the aforementioned features related to each technique (NIRAS in blue, and FANSIRAS in yellow), and the applied configuration (upward with solid lines, and downward with dashed lines), strong correlations among the trends obtained for every set of specimens are easily identified for the common upward and downward configurations.

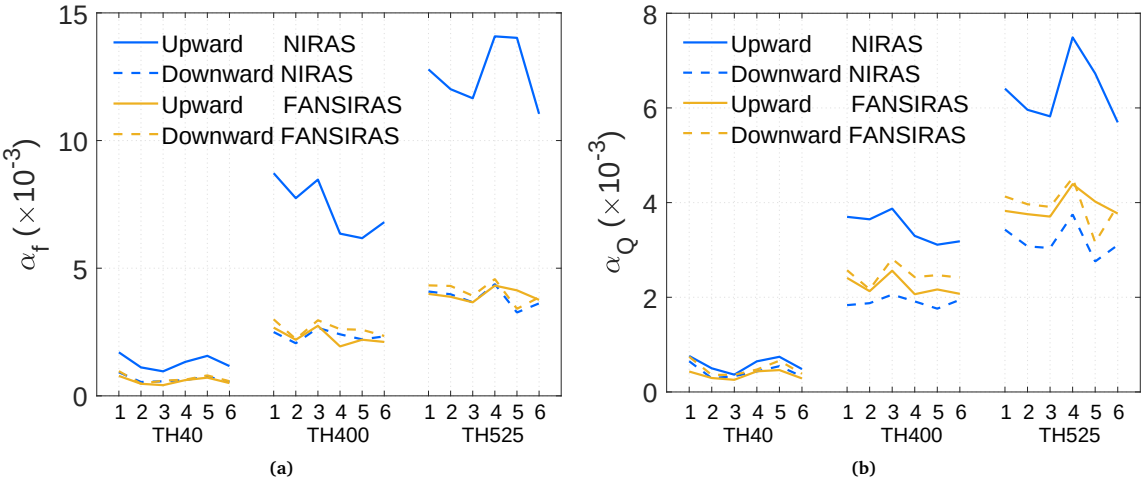

Figure 10: Results of the non-linear hysteretic parameters at different exposure temperatures, 40°C, 400°C and 525°C, computed by the NIRAS technique (blue lines) and the FANSIRAS technique (yellow lines) and for the two different analysed configurations: upward impact amplitudes (solid lines) and downward impact amplitudes (dashed lines). a) Amplitude-dependent frequency shift (α_f). b) Amplitude-dependent damping factor (α_Q).

A further data analysis is shown in Figure 11. Error bars depict the standard deviation of the set comprising the six α parameters computed for the six independent specimens at each damaging temperature. Circles and diamonds, denoting the upward and downward configurations respectively, represent the arithmetic mean of the aforementioned set. As discussed in the previous results, the test configuration in the impact resonance spectroscopy assessment plays an important role when quantifying the material's non-linear response. Note that the y-axis limits are set to be common in both figures. At first, a significant divergence of values was obtained by the NIRAS technique in the upward configuration for the other three assessments considered in the present study. Figure 11a shows the obtained equivalent distributions of α_f and α_Q for the FANSIRAS algorithm (upward and downward configurations) and the α_f estimated by means of NIRAS in the downward configuration. In Figure 11b, a slightly low-biased trend is observed for α_Q for the NIRAS downward configuration. This behaviour was

attributed to the narrower range of measurable amplitudes for the NIRAS technique. Thus Figure 11 could be interpreted to confirm that the FANSIRAS technique seemed robust not only different testing configurations, but also for both possible hysteretic parameters α_f and α_Q. FANSIRAS seemed capable of accurately characterising the microstructural degradation process by reproducing differentiated damage intervals and establishing a stabler assessment scenario.

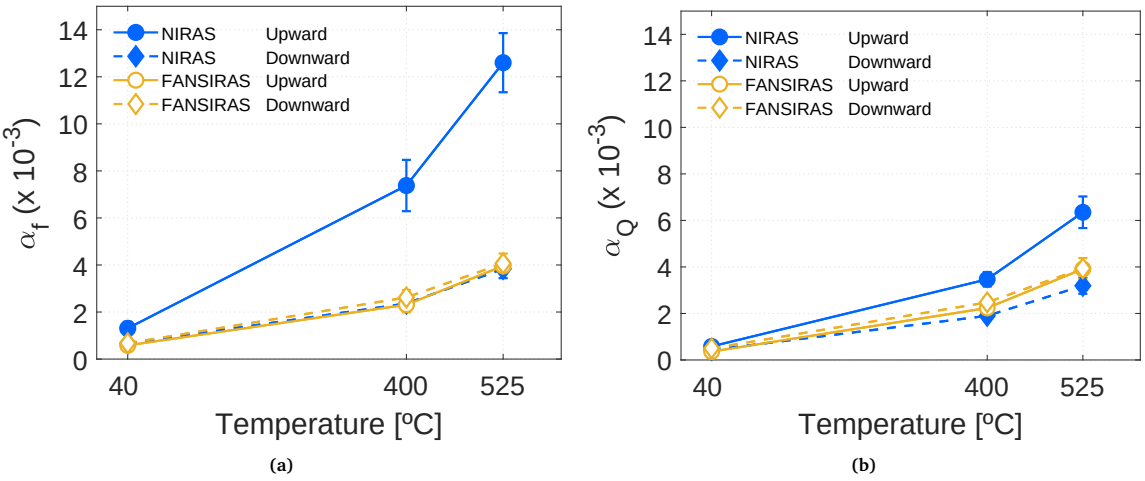

Figure 11: Results of the non-linear hysteretic parameters at different exposure temperatures, $40°C$, $400°C$ and $525°C$, computed by the NIRAS technique (circle markers) and the FANSIRAS technique (triangle markers) and for the two different analysed configurations: upward impact amplitudes (solid lines) and downward impact amplitudes (dashed line). Error bars depict the standard deviation of the set compromising six α parameters computed for six independent specimens at each exposure condition. a) Amplitude-dependent frequency shift (α_f). b) Amplitude-dependent damping factor (α_Q).

Following this line of thought, the Read ratio (α_Q/α_f) was analysed for the different algorithms and configurations (Figure 12). This ratio allowed comparisons to be made of the material's elastic and dissipative properties. For mortar, the elastic properties (α_f) seemed to vary more than the material's dissipation properties (α_Q), although the dissipation properties seemed to increase in sensitivity as the damage level of damage rose. The obtained values are consistent with those reported previously in the literature [3]. For NIRAS, two different trends related to the upward and downward configurations were identified (Figure 12a). When the specimen was relaxed, the elastic and damping properties seemed to behave more differently than in conditioning dynamic state: a trend that increased as the damage level rose. A similar trend to NIRAS in the downward configuration was found in the FANSIRAS results (Figure 12b). Note that a Read number that equals 1 verifies that fully conditioned specimens satisfy the purely quadratic non-linearity (Eq. 2). In the undamaged specimens, the absolute difference between ($\alpha_f - \alpha_Q$) was similar to damaged specimens' calculated value: 0.2 (see Table 1), but the expression of

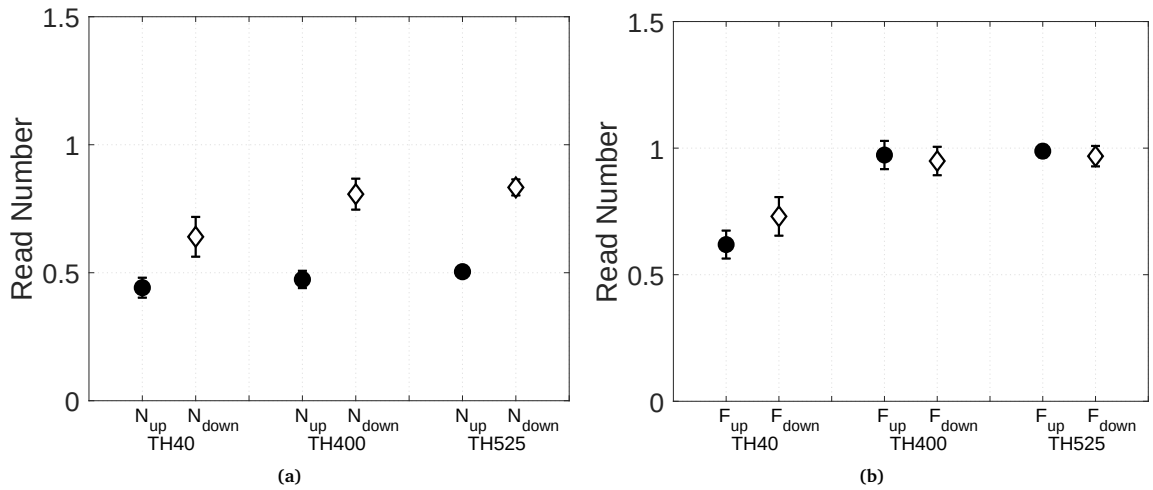

Figure 12: Read ratio results for the different configurations (up: upward, down: downward) and thermal damage levels (TH40, TH400, TH525). a) NIRAS (N) algorithm. b) FANSIRAS (F) algorithm.

the Read ratio enhanced its differences. The distinct trend between the upward and downward configurations suggested that stronger impacts might be needed to fully condition the undamaged specimens.

4.2.3. NDT measurements based on the area of hysteresis

The results shown in Figures 10 and 11 reveal that non-linear hysteretic measurements depend on the conditioning level of the test sample. In order to empirically quantify differences in on the non-linear hysteretic acoustic measurements caused by conditioning effects we propose that new alternative NDT parameters based on the hysteresis area computed from elastic and dissipative properties be considered.

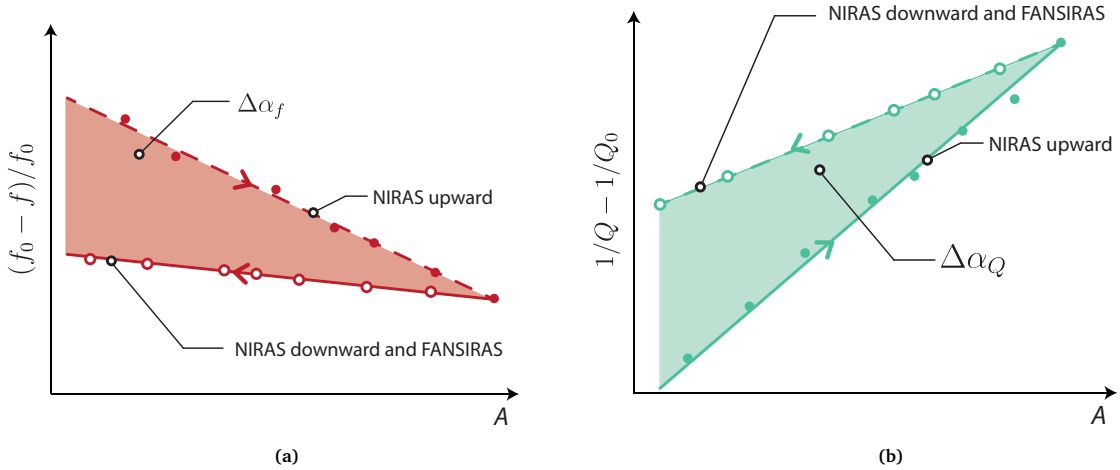

Figure 13: Graphical representation of the identified behaviour of the hysteretic non-linear parameters and the resulting so-called area of hysteresis. a) Area of hysteresis extracted from the resonance frequency shift parameter $\Delta\alpha_f$. b) Area of hysteresis extracted from damping properties parameter $\Delta\alpha_Q$.

Based on the aforementioned hypothesis, the alternative measurements represent the area of hysteresis computed from the elastic and dissipative properties: $\Delta\alpha_f$ and $\Delta\alpha_Q$. Both parameters can be computed from NIRAS upward and NIRAS downward (N-N, Eq. 18, 20), and from NIRAS upward and FANSIRAS upward (N-F, by assuming the equivalent results for FANSIRAS downward, Eq. 19, 21) and by attempting to hit the specimen the least number of times.

$$\Delta\alpha_f^{N-N} = \alpha_f^{NIR_{up}} - \alpha_f^{NIR_{down}} \tag{18}$$

$$\Delta\alpha_f^{N-F} = \alpha_f^{NIR_{up}} - \alpha_f^{FAN_{up}} \tag{19}$$

$$\Delta\alpha_Q^{N-N} = \alpha_Q^{NIR_{up}} - \alpha_Q^{NIR_{down}} \tag{20}$$

$$\Delta\alpha_Q^{N-F} = \alpha_Q^{NIR_{up}} - \alpha_Q^{FAN_{up}} \tag{21}$$

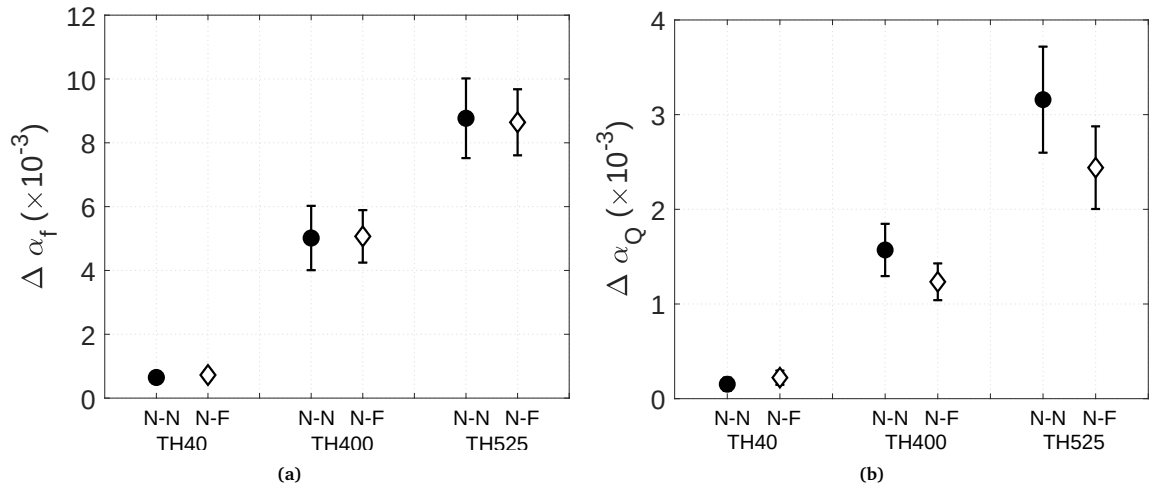

Figure 14: Results of the area of hysteresis shown by specimens at different exposure temperatures, $40°C$, $400°C$ and $525°C$. a) $\Delta\alpha_f$ computed for NIRAS upward and NIRAS downward (N-N), and NIRAS upward and FANSIRAS upward (N-F). b) $\Delta\alpha_Q$ computed for NIRAS upward and NIRAS downward (N-N), and NIRAS upward and FANSIRAS upward (N-F).

The obtained results are graphically represented in Figure 14. When analysing the behaviour of $\Delta\alpha_f$, the results obtained by both two ways of calculating the parameter were equivalent. However with $\Delta\alpha_Q$, slight

differences appeared due to the S-shape of the FANSIRAS estimation and the lower amplitude range of the NIRAS algorithm. In any case, both raised parameters were able to identify the damage level and open up an alternative way to characterise the damage level by means of the conditioning level found in the impact resonant acoustic spectroscopy experiments.

Beyond showing the potential of hysteresis parameters to quantify the damage level when specimens were not conditioned, these alternative NDT measures could also be used to determine the hypothetical unknown dynamic history of the specimen under study. For certain unknown conditioning, the FANSIRAS non-linear measure can detect the damage level, and the difference with NIRAS upward configuration data can illuminate the conditioning level.

5. Conclusions

This study analysed the differences between impact resonance spectroscopy methods NIRAS and FANSIRAS with tests done on thermally damaged mortar samples. The NIRAS tests were conducted using either sequentially increasing (upward) or decreasing (downward) load amplitudes. The upward and downward loading profiles allowed us to evaluate the slow dynamic and conditioning effects on non-linear spectroscopy techniques. The mortar samples were exposed to sustained temperatures of 40°C, 400°C and 525°C, and provided different thermal damage levels. This study revealed that the non-linear hysteretic parameters extracted by NIRAS, α_f^{NIR} and α_Q^{NIR}, differed between the upward and downward loading configurations. The FANSIRAS algorithm provided results from a single resonant signal, which were the equivalent results to NIRAS when the specimen was conditioned. The NIRAS results, according to the damage treatment, showed that the differences between the upward and downward series (or its equivalent by FANSIRAS) became bigger with increasing damage level. Based on this, new NDT proportional parameters to the area of hysteresis appeared, and demonstrated that the conditioning level was able to characterise the damage level.

Furthermore, after previously testing the specimen, both parameters α_f and α_Q obtained by NIRAS in the downward configuration and FANSIRAS were almost equivalent. The analysis of the Read number for each technique and each dynamic condition state demonstrated that the purely hysteretic quadratic non-linearity model satisfied the non-linear elastic behaviour when the material was conditioned. However, other models need

to be studied and proposed, to particularly account for the slow dynamics, conditioning and relaxation effects. The disrupting effects of slow dynamic conditioning on the NIRAS tests using the conventional upward loading configuration were significant. Erroneous conclusions about the damage level can be drawn if the previous relaxed or conditioned state of the specimen under study is not taken into account. The data analysed by the FANSIRAS algorithm remained largely unaffected by the slow dynamic or hysteretic effects.

Acknowledgements

This work has been supported by the Spanish Administration under grants BIA2014-55311-C2, BIA2017-87573-C2, BES2015-071469, PAID-10-19 and FEDER funds.

References

[1] R. A. Guyer, P. A. Johnson, Nonlinear Mesoscopic Elasticity: Evidence for a New Class of Materials, Physics Today 52 (4) (1999) 30.
[2] L. D. Landau, E. M. Lifshitz, Theory of Elasticity, Pergamon, Oxford, England, 3rd edn., 1986.
[3] P. Johnson, A. Sutin, Slow Dynamics and Anomalous Nonlinear Fast Dynamics in diverse solids, The Journal of the Acoustical Society of America 117 (1) (2005) 124–130.
[4] K. Van Den Abeele, J. Carmeliet, J. A. Ten Cate, P. Johnson, Nonlinear ElasticWave Spectroscopy (NEWS) Techniques to Discern Material Damage, Part I: Nonlinear Wave Modula- tion Spectroscopy (NWMS), Research in Nondestructive Evaluation 12 (1) (2000) 17–30.
[5] L. Ostrovsky, P. A. Johnson, Dynamic nonlinear elasticity in geomaterials, Rivista del Nuovo Cimento 24 (2001) 1–46.
[6] K. Van Den Abeele, P. A. Johnson, A. Sutin, Nonlinear Elastic Wave Spectroscopy (NEWS) Techniques to Discern Material Damage, Part II: Single-Mode Nonlinear Resonance Acoustic Spectroscopy, Research in Nondestructive Evaluation 12 (1) (2000) 17–30.
[7] J. Chen, A. R. Jayapalan, J. Y. Kim, K. E. Kurtis, L. J. Jacobs, Rapid evaluation of alkali–silica reactivity of aggregates using a nonlinear resonance spectroscopy technique, Cement and Concrete Research 40 (6) (2010) 914–923.
[8] C. Payan, T. J. Ulrich, P-Y. Le Bas, T. Saleh, M. Guimaraes, Quantitative linear and nonlinear resonance inspection techniques and analysis for material characterization: Application to concrete thermal damage, The Journal of the Acoustical Society of America 136 (2) (2014) 537–546.
[9] V. Genovés, L. Soriano, M. V. Borrachero, J. Eiras, J. Payá, Preliminary study on short-term sulphate attack evaluation by non-linear impact resonance acoustic spectroscopy technique, Construction and Building Materials 78 (2015) 295–302.
[10] J. N. Eiras, J. Monzó, J. Payá, T. Kundu, J. S. Popovics, Non-classical nonlinear feature extraction from standard resonance vibration data for damage detection, The Journal of the Acoustical Society of America 135 (2) (2014) EL82–EL87.
[11] U. Dahlen, N. Ryden, A. Jakobsson, Damage identification in concrete using impact non-linear reverberation spectroscopy, NDT & E International 75 (2015) 15–25.
[12] A. Carrión, V. Genovés, G. Pérez, J. Payá, J. Gosálbez, Flipped Accumulative Non-Linear Single Impact Resonance Acoustic Spectroscopy (FANSIRAS): A novel feature extraction algorithm for global damage assessment, Journal of Sound and Vibration 432 (2018) 454 – 469.
[13] M. Scalerandi, M. Bentahar, C. Mechri, Conditioning and elastic nonlinearity in concrete: Separation of damping and phase contributions, Construction and Building Materials 161 (2018) 208–220.
[14] M. C. Remillieux, R. A. Guyer, C. Payan, T. Ulrich, Decoupling nonclassical nonlinear behavior of elastic wave types, Physical review letters 116 (11) (2016) 115501.
[15] P. C. Aïtcin, Binders for durable and sustainable concrete, CRC Press, 2014.
[16] J. Marchand, I. Odler, J. P. Skalny, Sulfate attack on concrete, CRC Press, 2003.
[17] M. Alexander, S. Mindess, Aggregates in concrete, CRC Press, 2010.
[18] U. Schneider, Concrete at high temperatures - A general review, Fire Safety Journal 13 (1) (1988) 55–68.
[19] Q. Ma, R. Guo, Z. Zhao, Z. Lin, K. He, Mechanical properties of concrete at high temperature-A review, Construction and Building Materials 93 (2015) 371–383.
[20] V. Malhotra, N. Carino, Handbook on Nondestructive Testing of Concrete, Civil engineering, CRC Press, 2004.
[21] S. J. Park, H. J. Yim, H. G. Kwak, Nonlinear resonance vibration method to estimate the damage level on heat-exposed concrete, Fire Safety Journal 69 (2014) 36–42.
[22] V. Genovés, F. Vargas, J. Gosálbez, A. Carrión, M. Borrachero, J. Payá, Ultrasonic and impact spectroscopy monitoring on internal sulphate attack of cement-based materials, Materials & Design 125 (Supplement C) (2017) 46 – 54.
[23] K. J. Leśnicki, J. Y. Kim, K. E. Kurtis, L. J. Jacobs, Characterization of ASR damage in concrete using nonlinear impact resonance acoustic spectroscopy technique, NDT & E International 44 (8) (2011) 721–727.
[24] G.-K. Park, H. J. Yim, Evaluation of Fire-Damaged Concrete: An Experimental Analysis based on Destructive and Nondestructive Methods, International Journal of Concrete Structures and Materials 11 (3) (2017) 447–457.

[25] C. Payan, T. Ulrich, P. Le Bas, M. Griffa, P. Schuetz, M. Remillieux, T. Saleh, Probing material nonlinearity at various depths by time reversal mirrors, Applied Physics Letters 104 (14) (2014) 144102.
[26] C. Payan, V. Garnier, J. Moysan, P. Johnson, Applying nonlinear resonant ultrasound spectroscopy to improving thermal damage assessment in concrete, The Journal of the Acoustical Society of America 121 (4) (2007) EL125–EL130.
[27] H. J. Yim, J. H. Kim, S.-J. Park, H.-G. Kwak, Characterization of thermally damaged concrete using a nonlinear ultrasonic method, Cement and Concrete Research 42 (11) (2012) 1438–1446.
[28] V. Genovés, A. Carrión, D. Escobar, J. Gosálbez, J. Monzó, M. V. Borrachero, J. Payá, Nonlinear Acoustic Spectroscopy and Frequency Sweep Ultrasonics: Case on Thermal Damage Assessment in Mortar, Journal of Nondestructive Evaluation 38 (3) (2019) 61.
[29] K. Naugolnykh, L. Ostrovsky, Nonlinear wave processes in acoustics, Cambridge University Press, 1998.
[30] R. A. Guyer, P. A. Johnson, Nonlinear mesoscopic elasticity: the complex behaviour of rocks, soil, concrete, John Wiley & Sons, 2009.
[31] R. A. Guyer, K. R. McCall, G. N. Boitnott, Hysteresis, Discrete Memory, and Nonlinear Wave Propagation in Rock: A New Paradigm, Physical Review Letters 74 (1995) 3491–3494.
[32] M. F. Hamilton, D. T. Blackstock, et al., Nonlinear acoustics, vol. 237, Academic press San Diego, 1998.
[33] V. E. Gusev, Parametric acoustic source in a medium with hysteretic quadratic nonlinearity, in: AIP Conference Proceedings, vol. 524, AIP, 287–290, 2000.
[34] M. Muller, A. Sutin, R. Guyer, M. Talmant, P. Laugier, P. A. Johnson, Nonlinear resonant ultrasound spectroscopy (NRUS) applied to damage assessment in bone, The Journal of the Acoustical Society of America 118 (6) (2005) 3946–3952.
[35] K. Van Den Abeele, P. Y. Le Bas, B. Van Damme, T. Katkowski, Quantification of material nonlinearity in relation to microdamage density using nonlinear reverberation spectroscopy: Experimental and theoretical study., The Journal of the Acoustical Society of America 126 (3) (2009) 963–72.
[36] L. Cohen, Time-frequency analysis, vol. 778, Prentice Hall, 1995.
[37] J. A. TenCate, Slow Dynamics of Earth Materials: An Experimental Overview, Pure and Applied Geophysics 168 (12) (2011) 2211–2219.
[38] A. Novak, M. Bentahar, V. Tournat, R. El Guerjouma, L. Simon, Nonlinear acoustic characterization of micro-damaged materials through higher harmonic resonance analysis, Ndt & E International 45 (1) (2012) 1–8.
[39] T. A. Read, The internal friction of single metal crystals, Physical Review 58 (4) (1940) 371.
[40] C. Inserra, V. Tournat, V. Gusev, Characterization of granular compaction by nonlinear acoustic resonance method, Applied physics letters 92 (19) (2008) 191916.
[41] K. R. McCall, R. A. Guyer, Equation of state and wave propagation in hysteretic nonlinear elastic materials, Journal of Geophysical Research: Solid Earth 99 (B12) (1994) 23887–23897.
[42] R. Guyer, K. McCall, K. Van Den Abeele, Slow elastic dynamics in a resonant bar of rock, Geophysical Research Letters 25 (10) (1998) 1585–1588.
[43] J. A. TenCate, E. Smith, R. A. Guyer, Universal slow dynamics in granular solids, Physical Review Letters 85 (5) (2000) 1020.
[44] P. A. Johnson, A. Sutin, Nonlinear elastic wave NDE I. Nonlinear resonant ultrasound spectroscopy and slow dynamics diagnostics, in: AIP Conference Proceedings, 2005.
[45] M. Scalerandi, A. Gliozzi, C. Bruno, P. Antonaci, Nonequilibrium and hysteresis in solids: Disentangling conditioning from nonlinear elasticity, Physical Review B 81 (10) (2010) 104114.